Fibronectin fibers are highly tensed in healthy organs in contrast to tumors and virus-infected lymph nodes

Charlotte M. Fonta [a,1], Simon Arnoldini [a,1], Daniela Jaramillo [b], Alessandra Moscaroli [c], Annette Oxenius [b], Martin Behe [c] and Viola Vogel [a]

a - Laboratory of Applied Mechanobiology, *Institute of Translational Medicine, Department of Health Sciences and Technology, ETH Zurich, CH-8093 Zurich, Switzerland*
b - Institute of Microbiology, *ETH Zürich, CH-8093 Zurich, Switzerland*
c - Center for Radiopharmaceutical Sciences, *Paul Scherrer Institute, CH-5232 Villigen, Switzerland*

Correspondence to Viola Vogel: *viola.vogel@hest.ethz.ch*
https://doi.org/10.1016/j.mbplus.2020.100046

Abstract

The extracellular matrix (ECM) acts as reservoir for a plethora of growth factors and cytokines some of which are hypothesized to be regulated by ECM fiber tension. Yet, ECM fiber tension has never been mapped in healthy versus diseased organs. Using our recently developed tension nanoprobe derived from the bacterial adhesin FnBPA5, which preferentially binds to structurally relaxed fibronectin fibers, we discovered here that fibronectin fibers are kept under high tension in selected healthy mouse organs. In contrast, tumor tissues and virus-infected lymph nodes exhibited a significantly higher content of relaxed or proteolytically cleaved fibronectin fibers. This demonstrates for the first time that the tension of ECM fibers is significantly reduced upon pathological tissue transformations. This has wide implications, as the active stretching of fibronectin fibers adjusts critical cellular niche parameters and thereby tunes the reciprocal cell-ECM crosstalk. Mapping the tensional state of fibronectin fibers opens novel and unexpected diagnostic opportunities.

Introduction

Extracellular matrix (ECM) fibers are more than scaffolds to anchor cells [1]. While chemical cues presented by the ECM are well recognized drivers in organ development, tissue homeostasis, and, when altered, lead to the progression of various diseases [2], cells can actively change the chemical display of ECM fibers as protein stretching can turn molecular binding sites on or off [3]. Yet nothing is known so far at the tissue level about how much force cells apply to their neighbors and to ECM fibers, even though many studies suggested that the tensional state of ECM fibers might regulate cell and organ functions and be altered during pathological transformations such as in cancer [1,3–9]. Also, many questions remain unsolved about how stromal cells get reprogrammed upon pathological transformations, for example in a tumor stroma, and whether ECM fiber tension plays a significant role in those processes. Many studies reported tissue stiffening in tumor stroma, yet nothing was known about the tensional state of individual ECM fibers under healthy and diseased conditions, and whether changes of their tensional state might play a role in tumor progression [10]. While a wide range of micro- and nanotechnology tools were engineered in the last two decades to probe forces and the tensional state of individual ECM fibers in vitro and in cell culture [3,7,11,62], they cannot be applied easily to probe tissue ECM fiber tension. Even though the bulk stiffnesses of tissues have been widely probed, frequently via indentation [12,13], no tools were available until recently to map tissue ECM fiber tension at the molecular scale. No information is thus available on how alterations in the tensional state of ECM fibers might regulate tissue morphogenesis, homeostasis or pathological transformations. The urgency to learn how to translate the plentiful insights

in mechanobiology as obtained on single cells or in 2D cell cultures to the tissue level is potentiated by findings that ECM stiffness is progressively increasing for cancer [14,15] and for different fibrotic disorders [16,17], but also for lymph node swelling in response to acute inflammation [18–20]. We thus took advantage of a peptide probe recently developed in our lab [21–23] to map fibronectin fiber tension in selected healthy and diseased organs.

Fibronectin is one of the most abundant ECM proteins with binding sites for cells, bacteria and for a plethora of growth factors, cytokines and matrix molecules [1,3,24,25]. Several binding sites on fibronectin have been documented to be switched on or off by tensile forces, thus tuning their affinities [3,6,22,23,25–28]. The question thus arises whether an upregulated expression of fibronectin, and/or a change of the tensional state of fibronectin fibers has an impact on the local binding and availability of matrix-bound growth factors or cytokines, as well as on fibronectin-integrin interactions [3], and thus on cell adhesion, migration and differentiation [6,26,29], thereby steering the tissue response. This is of special interest considering the fact, that an increased expression and assembly of fibronectin fibers has been reported during embryogenesis and wound healing, as well as in many cancer types and in fibrotic tissues [1,5,30–35]. Increased cell contractility due to activation of fibroblasts into myofibroblasts [17,36], and altered composition and crosslinking of ECM have been identified as further hallmarks in cancer and fibrotic diseases and are associated with increased tissue stiffness [9,14,15]. Understanding the tensional signature of fibronectin fibers in healthy versus diseased tissues could potentially enable the development of a new generation of drugs that specifically target the tensional states of ECM proteins.

We recently introduced the bacterial adhesin-derived tension probe FnBPA5, originating from the cell-wall anchored adhesins of *S. aureus*, known to specifically bind to the N-terminus of fibronectin with high affinity. The FnBPA5 peptide targets fibronectin, but its binding affinity differentiates between tensional states of fibronectin fibers [21–23]. Steered molecular dynamics followed up by stretch assays revealed that the stretching of fibronectin fibers destroys FnBPA5's multivalent binding epitope [22,23]. We have shown in a previous study that our tension probe specifically binds to fibronectin and accumulates in tumor stroma in vivo [21]. Our fluorescently labeled Cy5-FnBPA5 tension probe thus offers a unique and novel approach to assess differences in the tensional state of fibronectin in specific tissues of interest. The big advantage of the peptide tension probes compared to our previously introduced fibronectin-FRET sensors [3,11] is that they can be used to stain tissue cryosections from any organ of interest [21], while the fibronectin-FRET sensors have to be added to the medium of a living cell culture such that cells can actively incorporate them into their own ECM [3,11]. This peptide tension probe is also well suited for in vivo applications to target tissues with a high content of structurally relaxed fibronectin fibers [21]. Notice though that the Cy5-FnBPA5 tension probe cannot distinguish whether tensed tissue fibers relax because the cells apply less force or because they are enzymatically cleaved, as both scenarios lead to the presentation of the structurally unperturbed equilibrium epitope with high affinity binding of FnBPA5. As a consequence of the low molecular weight of the FnBPA5 peptide compared to antibodies and the lack of secondary structure, superior tissue penetration properties are expected [37], thus offering significantly more insights as previously presented by phage-based probes, for which neither exact binding mechanism, corresponding epitopes nor binding affinities are known [38]. Assessing the fibronectin fiber tension in healthy organs is essential to establish the benchmark of what can be expected under homeostatic conditions, in contrast to ECM fiber tension alterations that are associated with pathological tissue transformations, as well as with tissue repair processes after injury or caused by infection.

We thus investigated cryosections of healthy organs versus tumor tissues and asked in addition how lymph node swelling upon viral infection or CpG adjuvant injection, might affect the tensional state of its fibronectin fibers. The lymphocytic choriomeningitis virus (LCMV) was chosen as a model for acute viral infections [39]. We used the FnBPA5-derived tension probe together with, both, immunohistochemistry of the myofibroblastic marker alpha smooth muscle actin (α-SMA), and label-free imaging of thick collagen I bundles with second harmonic generation (SHG), to better understand whether myofibroblastic differentiation and thickening of collagen I fibrils – as previously reported for fibroblasts in cancer [36] and fibrotic tissues [16,17,40] – might be influencing factors altering fibronectin fiber tension and thus FnBPA5 binding to cryosections from different organs. In both tumor tissues and in LCMV-infected lymph node sections, drastic alterations of fibronectin fiber strain were found compared to healthy organs and naïve lymph nodes. This study thus presents the first comparative ex vivo characterization of ECM fiber tension in healthy and pathologically transformed organs.

Results

After validating specific binding of our peptide probe to relaxed fibronectin in PC-3 tumor xenograft tissue in our last study [21], we now utilized the same Cy5-FnBPA5 tension probe to assess, for the first time, the mechanical strain of fibronectin fibers within cryosections of selected healthy versus diseased mouse

tissues, as well as in naïve versus swollen lymph nodes after LCMV infection or CpG adjuvant injection.

Fibronectin fibers are highly stretched in ECM of healthy organs and are significantly more relaxed in tumor stroma

In order to compare how fibronectin's tensional state differs in healthy versus diseased tissues, we probed cryosections from 8 weeks old CD1 nude mice. We proceeded to immunohistochemistry (IHC) to detect total fibronectin with a polyclonal fibronectin antibody. Our fluorescently-labeled tension probe Cy5-FnBPA5 was applied to visualize structurally relaxed fibronectin fibers in cryosections from healthy kidney, lung, heart and liver, as well as in cryosections from different tumor xenografts developed from the subcutaneous injection of either human lung adenocarcinoma cell line (SW2) or human ovarian carcinoma cell line (Skov3ip). A polyclonal antibody was chosen here, since fiber stretching can destroy some epitopes of monoclonal antibodies as well [3]. While all organs, healthy and diseased, show fibronectin ECM throughout when stained with a polyclonal anti-fibronectin antibody, most of these fibronectin fibers did not stain positively for Cy5-FnBPA5 (Fig. 1). In the healthy organs, little Cy5-FnBPA5 peptide binding was observed in representative lung, heart and liver sections, even though all sections showed a strong fibronectin signal. This suggests that most fibronectin fibers in these healthy cryosections are under high tension, with binding epitopes for the FnBPA5 peptide being altered or destroyed (Fig. 1). Significant Cy5-FnBPA5 binding was detected in the kidney, mostly in glomerular structures. Mouse glomeruli have been reported to have a diameter of around 80 μm [41], and thus correspond to the size of the structure observable in the zoomed-in images of kidney tissues in Fig. 1. As glomeruli filter blood, and since we know that FnBPA5 binds to its mechanically unstretched epitope in plasma fibronectin as it circulates in the blood as well [21], this observation is not unexpected. Quite strikingly, and in contrast to the healthy organs, tumor tissues showed rather heterogeneous and fiber-like Cy5-FnBPA5 staining exhibiting regions of significantly higher peptide binding (Fig. 1 & Supplementary Fig. S1), in agreement with our previous report [21]. This suggests that regions within this tumor stroma, unlike sections from healthy organs investigated here, show a significant higher proportion of fibronectin fibers with relaxed fibronectin conformations as they enabled high affinity binding of Cy5-FnBPA5.

Cy5-FnBPA5 binding to tumor ECM increases in proximity of myofibroblasts

As previously reported for fibroblasts in cancer [9,36] and fibrotic organs [16,17,35,40], activation of fibroblasts to α-SMA positive myofibroblasts – cancer-associated fibroblasts (CAFs) in tumor – is known to be upregulated in tumor tissues, as well as cellular contractility and ECM production [4,5,9,16,35,36,42]. Following up on our previous finding, where an increased presence of α-SMA was found around FnBPA5-detected relaxed fibronectin fibers in a PC-3 tumor xenograft cryosection [21], we next asked how the presence of myofibroblasts might affect the tensional homeostasis of ECM fibers, and whether the presence of myofibroblasts coincides with changes in the tensional states of fibronectin fibers also for different tumor mouse models. α-SMA expression is a well-documented marker for myofibroblasts and smooth muscle cells. It has been linked to increased cell contractility [40] and an overall stiffening of tissues [14,15], and was here visualized by IHC with a polyclonal α-SMA antibody. In the cryosections from healthy organs such as heart, kidney, liver and lung, the morphology and localization of α-SMA suggest that α-SMA is solely expressed by smooth muscle cells in the vascular walls of blood vessels, but not by CAFs/myofibroblasts. Moreover, only very little Cy5-FnBPA5 binding can be observed in the healthy organs, but not nearby the α-SMA expressing cells (Fig. 2A). In cryosections from SW2 and Skov3ip tumor xenografts, binding of Cy5-FnBPA5 to ECM fibers in the proximity to α-SMA expressing cells is clearly visible, and the morphology of α-SMA stains depicts elongated actin fibers (Fig. 2A). The localization and morphology of α-SMA in tumors differ substantially compared with healthy organs. A spatial proximity analysis to quantify the amount of α-SMA positive pixels surrounding every Cy5-FnBPA5 positive pixel in a 3×3 pixel array (see schematic Supplementary Fig. S2) revealed major correlations (Fig. 2C). For the healthy organs, only between 1% to 30% in average of all α-SMA positive pixels are within a distance of 0.4 μm or less to at least one pixel of Cy5-FnBPA5 (Fig. 2C). For the two tumor xenografts, in average 65% of all α-SMA pixels are in proximity with one or more Cy5-FnBPA5 pixels, which is significantly more than for healthy organs tissues ($p < 0.001$). Altogether, these results (Fig. 2A and C), depicting an increased binding of Cy5-FnBPA5 to relaxed fibronectin fibers in close proximity to α-SMA expressing myofibroblasts, confirm a role of myofibroblasts in the relaxation of fibronectin fibers in tumor stroma.

Relaxed fibronectin is found in proximity of thick collagen fibers

Thicker bundles of collagen fibers can be detected label-free, as they lead to nonlinear optical SHG. SHG originates from the helicity of non-centrosymmetric biological molecules and proteins [43], thus primarily originating from type I collagen bundles in biological tissues [44]. As tumor stroma is widely associated with

remodeled and stiffer ECM, rich in dense collagen I fibers [14] as compared to healthy tissue, and as our preliminary observations suggest increased relaxation of fibronectin fibers in tumor stroma, we next interrogated how dense collagen I bundles spatially correlate with structurally relaxed fibronectin fibers in tumor and healthy organs mouse cryosections. We added our fluorescently labeled tension probe to healthy and tumor mouse tissue sections. The SHG signals in these tissues were imaged with a multiphoton microscope and the Cy5-FnBPA5 signals with a confocal microscope. In healthy organs cryosections, very little to no SHG signal was detected, except in the lung where a strong SHG signal was detected, but no Cy5-FnBPA5 was detected in close proximity to this SHG signal (Fig. 2B). The alveoli of the lungs endure

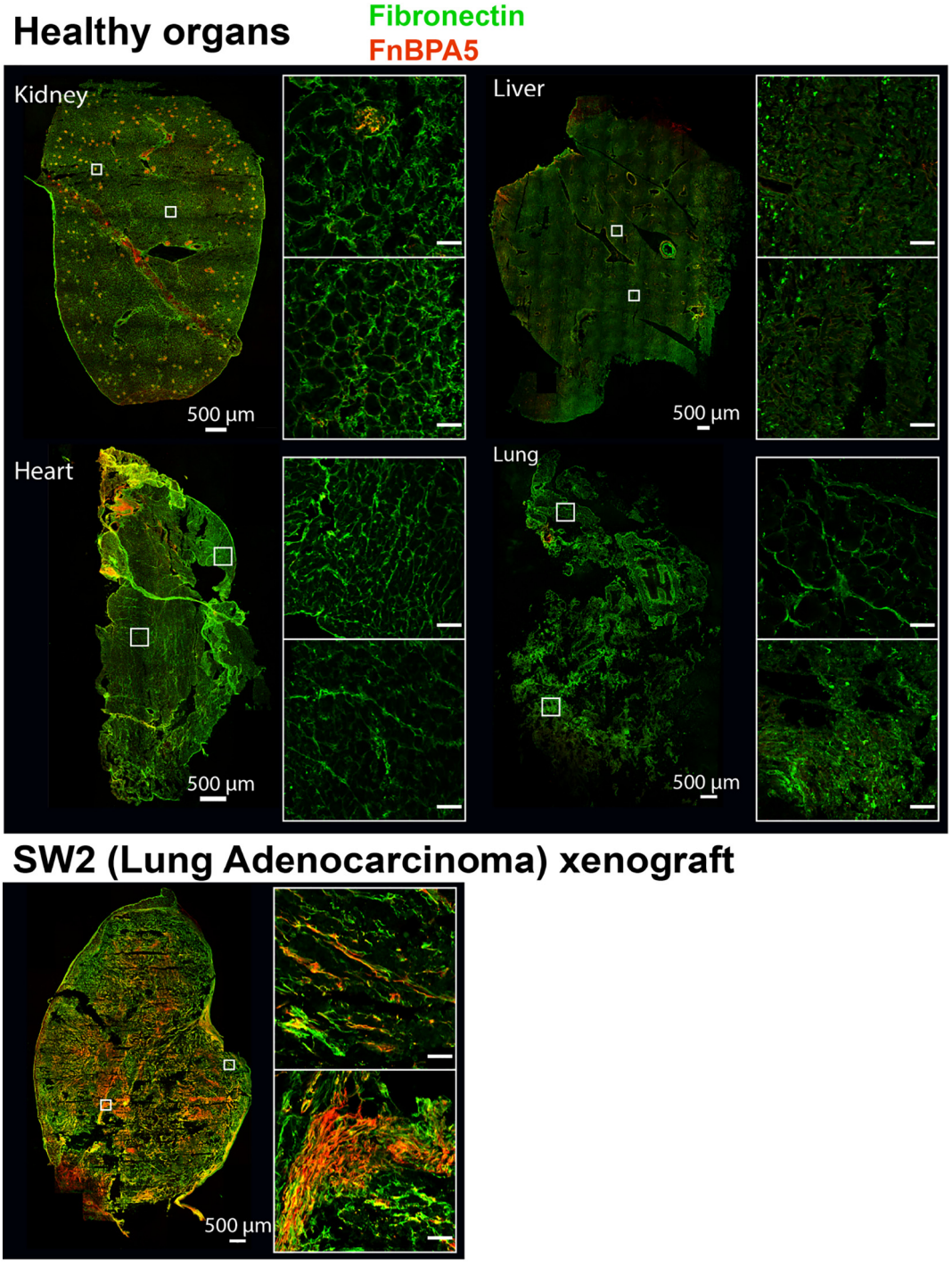

sustained mechanical deformation during respiration, which could explain the wavy aspect of the collagen I fibers detected by SHG, as previously observed [45]. In tumor tissue sections, the Cy5-FnBPA5 positive pixels were found in close proximity to dense collagen I fibers detected by SHG (Fig. 2B). A spatial proximity analysis revealed that, for the healthy heart and lung, only an average of 1% of the SHG pixels were detected in a close proximity to Cy5-FnBPA5 positive signals, while 10% in average of the SHG pixels were close to Cy5-FnBPA5 positive pixels for the healthy liver (Fig. 2D). The Cy5-FnBPA5 signal is highly heterogeneous throughout the kidney as mainly localized in the glomeruli, rich in unstrained plasma fibronectin. However, we did not expect to detect more collagen I fibers in these kidney structures. Hence, to avoid averaging out a potential preferred spatial proximity of collagen I fibers to Cy5-FnBPA5, either in the glomeruli or outside the glomeruli, the spatial proximity analysis was run on both glomeruli-only pixels and non-glomeruli pixels in the kidney images. In average 4% of the total SHG detected in the glomeruli was within 0.4 μm to at least one pixel of Cy5-FnBPA5, hence confirming the absence of dense collagen I fibers bundles in healthy kidney glomeruli. In the kidney stroma without glomeruli, up to 24% of the SHG pixels detected are in close proximity to at least one pixel of Cy5-FnBPA5, which is still significantly less than in the tumor tissues (Fig. 2D). Indeed, for the tumor xenografts, about 35% for SW2 and 45% for Skov3ip of the SHG pixels are within a 0.4 μm distance of at least one Cy5-FnBPA5 positive pixel (Fig. 2D). These spatial proximity results suggest an increased spatial correlation between dense collagen I fibers and structurally relaxed fibronectin in tumor xenografts tissue sections compared to the healthy organs investigated here.

Viral infection, but not adjuvant stimulation, reduces fibronectin fiber tension in lymph nodes

Next, we asked whether lymph nodes, organs known to swell significantly while fighting infections, would show significant alterations in the fibronectin fibers strain of their ECM. Lymph node swelling is tightly associated with the ability of our immune system to fight infections, the mechanisms regulating these drastic tissue expansions are only since recently in the focus of investigations [18,19]. Net cell influx and proliferation of immune cells during an immune response lead to a fast increase in lymph node size [20]. Resident lymph node fibroblastic reticular cells (FRCs) are responsible for the assembly and maintenance of the collagen-rich lymph node reticular fiber networks and lose contractility during infection which is currently thought to allow lymph node expansion [18–20]. The schematic in Fig. 3B shows the lymph node architecture together with the B cell follicles and T cell zone with reticular network assembled by FRCs. To test the impact of lymph node swelling on fibronectin fiber tension within lymph node reticular networks, we used lymph nodes from mice either infected with lymphocytic choriomeningitis virus (LCMV) or treated with CpG adjuvant, using naïve lymph nodes as controls. For this, groups of three wild-type C57BL/6 mice were injected into the right footpad with either PBS, 200 FFU of LCMV or 5 μg CpG and sacrificed 8 days after injection (Fig. 3A). Popliteal lymph nodes as draining lymph nodes next to the injection site were extracted and weighed (Fig. 3C). LCMV treated lymph nodes exhibited a five-fold weight increase ($p < 0.01$) compared to naïve control lymph nodes. Lymph nodes from CpG treated mice also showed a trend of weight increase.

The extracted lymph nodes were further frozen, sectioned and stained with a polyclonal fibronectin antibody, to visualize the presence of all fibronectin fibers, and with a reticular cell and fiber marker ER-TR7 antibody to visualize the reticular fiber network that extends throughout the lymph node. Our tension probe Cy5-FnBPA5 was also added to visualize structurally relaxed fibronectin fibers in these lymph nodes tissues. A scrambled Cy5-FnBPA5 derivative was used as negative control showing no specific binding to the ECM of tissues investigated here (Supplementary Fig. S3). Reticular networks as visualized by ER-TR7 antibody staining that binds to FRC and reticular fibers, are clearly visible in all samples (Fig. 3). Importantly, while Cy5-FnBPA5

Fig. 1. Mapping the fibronectin fiber tension in cryosections of selected healthy and diseased mouse organs. Cryosections from healthy heart, kidney, liver and lung and sections from SW2 tumor xenograft model were stained with a fibronectin polyclonal antibody (green, abcam, ab23750) as well as with the tension-sensitive peptide Cy5-FnBPA5 (red). Cy5-FnBPA5 binds with nM affinity specifically to relaxed fibronectin fibers and with less affinity to stretched fibronectin fibers whose binding epitope gets altered or even destroyed when stretched [21–23]. Cryosections of healthy hearts, livers and lungs all show the existence of an elaborate fibronectin fibril network, yet very little to no specific Cy5-FnBPA5 binding, indicating that the majority of fibronectin fibers exists in highly stretched conformations. Partial tissue detachment at the upper left corner of the heart cryosection caused some Cy5-FnBPA5 non-specific accumulation in the tissue folds, creating a Cy5-FnBPA5 signal artifact. Healthy kidney cryosections also show some binding of Cy5-FnBPA5 in glomeruli since FnBPA5 can also bind to soluble fibronectin [21]. Cryosections from SW2 tumor xenograft depict a highly heterogeneous and fiber-like binding of Cy5-FnBPA5 to fibronectin, with strong Cy5-FnBPA5 signals in some but not all observed regions. Scale bar full sections: 500 μm; scale bar zoomed-in images: 50 μm.

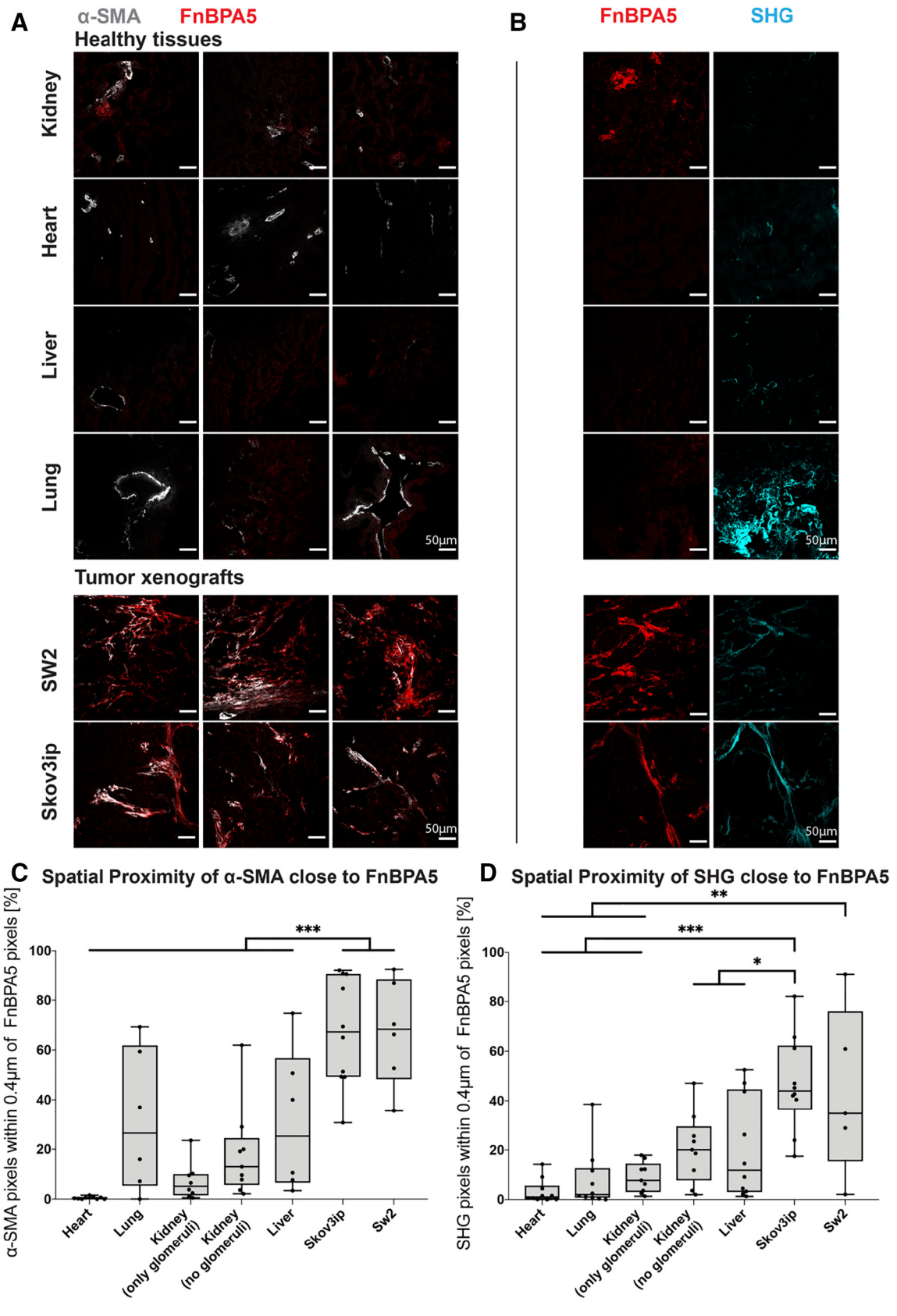
A
α-SMA
FnBPA5
Healthy tissues
Kidney
Heart
Liver
Lung
50µm
Tumor xenografts
SW2
Skov3ip
50µm
B
FnBPA5
SHG
50µm
50µm
C
Spatial Proximity of α-SMA close to FnBPA5
α-SMA pixels within 0.4µm of FnBPA5 pixels [%]
***
Heart
Lung
Kidney (only glomeruli)
Kidney (no glomeruli)
Liver
Skov3ip
Sw2
D
Spatial Proximity of SHG close to FnBPA5
SHG pixels within 0.4µm of FnBPA5 pixels [%]
**
***
*
Heart
Lung
Kidney (only glomeruli)
Kidney (no glomeruli)
Liver
Skov3ip
Sw2

binding was not detected in naïve and adjuvant swollen lymph nodes, binding of Cy5-FnBPA5 was exclusively seen for the virus-infected lymph node sections (Fig. 3E). These findings from the overview tissue sections were confirmed with zoomed-in images at different spots within the lymph node sections: they show Cy5-FnBPA5 binding only in lymph nodes from LCMV treated mice showing heterogeneities in binding between different lymph node zones (Fig. 3G, H, I). Additionally, co-staining for collagen I with a polyclonal collagen I antibody and Cy5-FnBPA5 confirmed the higher binding of our tension probe to swollen lymph nodes of LCMV-treated mice and furthermore showed presence of collagen I in the lymph nodes reticular network as previously reported [46] (Supplementary Fig. S4).

Discussion

Since nothing is known at the tissue level about how ECM fiber tension might co-regulate tissue homeostasis, or change in inflammation, cancer and other diseases, we addressed here for the first time whether fibronectin fibers are more stretched in healthy versus cancer and inflamed tissues. By utilizing our recently validated fibronectin fiber tension probe Cy5-FnBPA5, whose multivalent binding motif on fibronectin gets destroyed by stretching fibronectin [21–23], we discovered that fibronectin fibers are kept under high tension by the residing stromal cells in the healthy mouse lungs, heart, liver, kidneys and naïve lymph nodes, as fibronectin fibers stained positive for the polyclonal fibronectin antibody, but not for the tension probe Cy5-FnBPA5 (Figs. 1–3). A small Cy5-FnBPA5-positive signal was observed though in glomeruli in kidney tissue sections (Figs. 1 and 2). As the blood is filtered in the glomeruli, where the Cy5-FnBPA5 peptide can bind to blood circulating plasma fibronectin too [21], this finding is to be expected. In contrast, large patches of Cy5-FnBPA5-positive pixels are found in tumor tissues from SW2 and Skov3ip xenografts (Figs. 1 and 2) and in swollen lymph nodes upon acute viral infection (Fig. 3). The finding of relaxed fibronectin fibers in tumor tissues does not seem dependent on the mouse tumor model, as it agrees with our previous findings on a murine PC-3 (prostate carcinoma) xenograft model [21], and as reproduced in the present study with Skov3ip, SW2 and PC-3 tumor models (Figs. 1 and 2, Supplementary Figs. S1, S5 and S6). We thus conclude that, regardless of the tumor model, the reciprocal cell-ECM interactions drive malignant ECM transformations and perturb the highly stretched fibronectin ECM architecture. An increased binding of Cy5-FnBPA5 occurs also in swollen lymph nodes, but only after LCMV infection (Fig. 3), suggesting that large areas of these inflamed tissues contain a significant fraction of structurally relaxed fibronectin fibers. In agreement with our previous findings [21], thick bundles of collagen I fibers as detected with SHG were in close proximity to fibronectin fibers stained with the Cy5-FnBPA5 probe in cancerous tissues (Fig. 2). These same tissue regions rich in relaxed fibronectin fibers were found in the surrounding of myofibroblasts as probed by α-SMA immunostaining (Fig. 2). Vice versa, Cy5-FnBPA5 binding is not prominent in regions within the tumor tissue that lack α-SMA positive cells (Fig. 2).

The significantly higher content of structurally relaxed fibronectin fibers in tumor stroma is surprising and highly unexpected. This finding is remarkable since increased tissue stiffness and upregulation of cell contractility in CAFs, as observed via α-SMA expression and other measures [36,42,47], was generally believed to lead to more highly strained ECM fibers [15,32,36]. Most studies that described ECM stiffening in cancer focused on collagen fiber crosslinking into dense fibrils which was shown to promote tumor growth and metastasis [15,48,49]. It was often suggested, but not experimentally confirmed due to the lack of tension probes, that fibronectin fibers in tumor are more stretched, thereby potentially activating the release of Transforming Growth Factor-beta (TGF-β) [42]. The finding of large regions of relaxed fibronectin fibers in tumor stroma next to α-SMA positive cells might result from the fact that myofibroblasts upregulate collagen fiber assembly in their environment, as confirmed in murine tumor xenografts by SHG [21],

Fig. 2. Higher content of structurally relaxed fibronectin in proximity to α-SMA positive myofibroblasts and to dense collagen I bundles in tumor stroma compared to healthy organs. (A) Cryosections from healthy organs and tumor xenografts were stained with Cy5-FnBPA5 (red) and polyclonal α-SMA antibody (grey, abcam, ab5694). Representative images of tissue sections from healthy organs show expression of α-SMA in vessel walls accompanied by very little and unspecific Cy5-FnBPA5 binding. The α-SMA detected is mostly produced by smooth muscle cells of the vascular walls and does not colocalize with Cy5-FnBPA5 binding. Representative images of SW2 and Skov3ip tumor cryosections show a clear tendency of higher binding of Cy5-FnBPA5 adjacent to α-SMA expressing cells. (B) Dense collagen I fibers were detected by second harmonic generation (SHG) (cyan). Little SHG signal was detected in healthy organs with a very low proximity correlation observed between dense collagen I fibers and relaxed fibronectin fibers. In tumor xenografts tissues, dense collagen I fibers detected by SHG showed to be in close proximity to relaxed fibronectin fibers as detected with Cy5-FnBPA5. Scale bar: 50 μm. (C–D) Spatial proximity analysis of positive (C) α-SMA pixels and (D) SHG pixels above a threshold within a 3 × 3 pixel matrix surrounding every Cy5-FnBPA5 positive pixel (1 μm = 2.8050 pixels). ***$p < 0.001$, **$p < 0.01$, *$p < 0.05$.

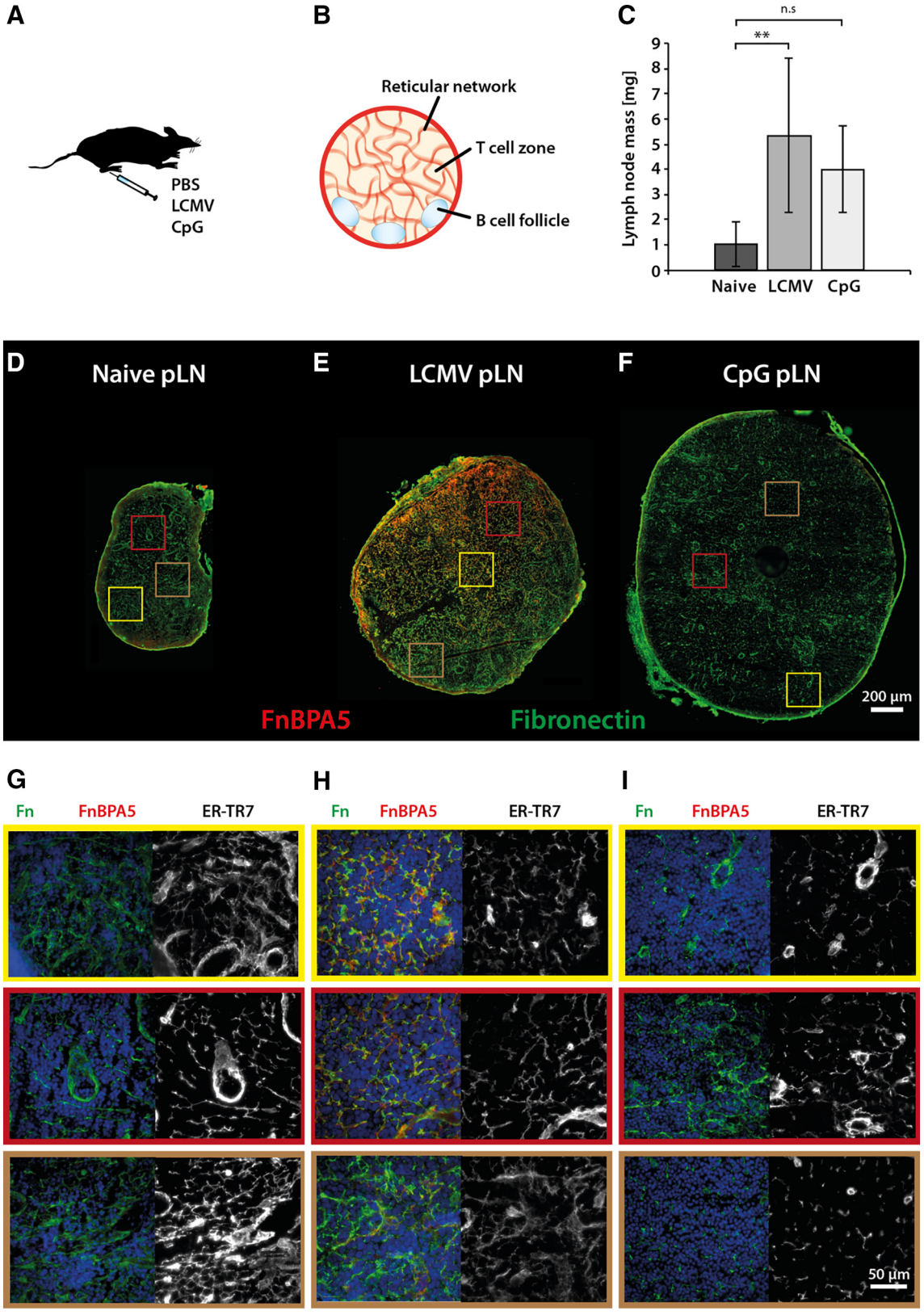
A
PBS
LCMV
CpG
B
Reticular network
T cell zone
B cell follicle
C
n.s
**
Lymph node mass [mg]
0
1
2
3
4
5
6
7
8
9
Naive
LCMV
CpG
D
Naive pLN
E
LCMV pLN
F
CpG pLN
FnBPA5
Fibronectin
200 µm
G
H
I
Fn
FnBPA5
ER-TR7
50 µm

and/or that an upregulated content of collagen fibers might reduce the tensional state of fibronectin fibers as previously shown in cell culture [28,50]. Another influencing factor could be the increased presence and activity of proteolytic enzymes such as MMPs, known to efficiently disturb the mechanical connectivity of ECM fibers in tumor tissues [15,50,51]. Given the reciprocal cell-ECM interactions [2,3], future research furthermore has to reveal whether and how changes of fibronectin fiber tension in microenvironmental niches might induce phenotypic alterations of tissue residing cells.

It is also remarkable that the swelling of lymph nodes as induced by adjuvants does not result in a measurable change of the tension of fibronectin fibers (Fig. 3). Here we find that fibronectin fibers are under high tension in both, naïve and CpG adjuvant-swollen lymph nodes (Fig. 3). The fibronectin-ensheathed lymph node collagen-rich conduit fibers are assembled by FRCs, and are known to support the migration of lymphocytes, dendritic cells (DCs) and small lymph-borne antigens along the collagen-rich conduits [46,52]. Fibroblasts assemble highly stretched fibronectin fibers when seeded on protein-coated flat substrates, or on electrospun silk fibers [53]. Also, when collagen-encapsulated fibroblasts contract their surrounding gel, they moved from the interior to the surface of the microgels, where they again assemble a highly tensed fibrillar fibronectin matrix [7]. The fibronectin fibers are also more tensed in newly assembled ECM by fibroblast or mesenchymal stem cells when seeded on rigid versus soft substrates [29,54]. Our finding that FRCs assemble highly stretched fibronectin fibers on lymph node conduits, even in the naïve state, could thus be explained by the rigidity of the collagen-rich conduit surfaces.

Even though lymph node swelling involves the downregulation of FRCs contractility by the action of C-type Lectin Receptor (CLEC-2) [5,18–20], it was unclear whether to expect that fibronectin fibers within naïve or swollen lymph nodes are kept under high or low tensional homeostasis. Lymph node swelling is intimately linked to the staging of an innate immune response. The expansion of the lymph node upon the onset of an immune response results from an increased T cell proliferation and increased cellularity caused by the entry of naïve lymphocytes into the lymph node [19,20]. Lymph node swelling is accompanied by fibroblastic reticular network expansion and decreased actomyosin-driven contractility of the FRCs caused by upregulated expression of CLEC-2 by migratory DCs, stromal cells of the lymph node and FRCs [18,19]. Indeed, in homeostatic conditions, Podoplanin (PDPN) activates the RhoA/C and Myosin II–mediated FRCs contractility by promoting actomyosin contractility. The upregulated CLEC-2 upon inflammation is thought to counteract PDPN activity, thus decreasing the actomyosin-driven FRCs contractility to enable lymph node expansion [18,19]. While one could expect that a decrease in cell contractility would result in a lowered fibronectin fiber tension in lymph node swelling, here we observed two different outcomes in regards of fibronectin fiber tension upon inflammation caused by either a virus infection or a mere CpG adjuvant stimulation. Indeed, lymph node swelling as induced here by a viral infection with LCMV causes a significantly higher binding of Cy5-FnBPA5 (Fig. 3E, H) in contrast to CpG adjuvant-induced swelling (Fig. 3F, I) or the untreated, naïve control (Fig. 3D, G). While the treatment with adjuvants, such as oligonucleotides containing CpG motifs, is known to results in an increased lymph node size, while maintaining the FRCs network's structure and function [55,56], LCMV infection results in a $CD8^+$ T-cell mediated destruction of the FRCs network, resulting in a depletion of contractile FRCs within infected lymph nodes [18–20,39]. Here we now show that LCMV infection results in a measurable relaxation of the reticular fibronectin fiber network in the draining lymph nodes at day 8 after viral infection (Fig. 3E, H), perhaps induced by proteolytic ECM cleavage.

Could there be a physiological role of fibronectin fiber stretching under healthy conditions, or of cleaved and thus relaxed fibronectin fiber fragments during viral infections? As fibronectin contains many binding sites for growth factors, cytokines and other ECM molecules, stretching of fibronectin fibers might expose some of those binding sites, while destroying others [3]. Interleukin-7 (IL-7), a fibronectin-binding cytokine, is a

Fig. 3. Higher binding of Cy5-FnBPA5 in virally-infected lymph nodes than in naïve and CpG adjuvant-stimulated lymph nodes. (A) Experimental setup: Mice were injected with PBS, LCMV virus or CpG adjuvant solution. (B) Lymph nodes consist of a T-cell zone, a B-cell zone and a reticular network assembled by FRCs. (C) Weight of popliteal lymph nodes 8 days after treatment shows significant increase in lymph node mass in LCMV ($p < 0.01$) and a non-significant weight increase in CpG treated mice ($p = 0.123$). (D), (E), (F) Tissue sections of popliteal lymph nodes from differently treated mice immunostained with fibronectin polyclonal antibody (green, abcam, ab23750), Cy5-FnBPA5 (red), DAPI (blue). (D) In naïve popliteal lymph node section, fibronectin is present in the reticular network, but no significant binding of Cy5-FnBPA5 occurs. (E) In popliteal lymph node of a virally-infected (LCMV) mouse, binding of Cy5-FnBPA5 colocalizing with fibronectin in the reticular fibers is significantly enhanced. (F) In popliteal lymph node of a CpG-treated mouse, no binding of Cy5-FnBPA5 and a drastic decrease in density of reticular fibers due to lymph node swelling is seen. (G), (H), (I) Higher resolution zoomed-in images of respective areas in D,E,F with DAPI stain (blue) alongside with staining from reticular fiber marker ER-TR7 (grey, abcam, ab51824) and all fibronectin.

required factor for T cell homeostasis [57] and thus plays a central role in the adaptive immune system. Different from most other cytokines, IL-7 does not lead to T-cell activation, but is known to provide continuous signals to resting naïve and memory T cells in lymph nodes, where it upregulates their proliferation and differentiation as well as maintains the homeostasis of mature memory T-cells [19,58]. Importantly, IL-7 is more potent in the ECM-bound state compared to its soluble counterpart [59], which can explain that it displays these immune regulatory effects already at pM concentrations. We could recently show in an in vitro stretch assay that IL-7 binding to fibronectin is upregulated when stretching fibronectin fibers [25]. As IL-7 binding to fibronectin promotes T-cell adhesion [39,59], our data now suggest that keeping fibronectin fibers under tension in naïve and adjuvant-swollen lymph nodes enhances the bioavailability of ECM-bound IL-7 and thus the retention of T-cells in the lymph node. In contrast, viral infections that destroy the integrity and interconnectivity of the lymph node ECM fibers should lead to proteolytic fibronectin fiber cleavage and thus a structural relaxation of the fibers, and we postulated that this will lead to a release of ECM-bound IL-7 [25]. This proposition is supported by experimental, but so far not explained observations: an inverse correlation between the number of circulating peripheral T cells and blood IL-7 levels has been shown for viral HIV infections in humans [57]. Upon viral infection and CD8+ T cell activation, the FRC-assembled ECM network is destroyed, which results in both the relaxation of fibronectin fibers – as a result of the loss of contractile strain applied by FRCs – and hence the decrease of IL-7 bound to ECM, which triggers lymphocytes T cell activation. Finally, at the conclusion of an infection, after the initial swelling of the lymph node, the FRCs start to stretch again in order to avoid FRCs' network disruption, which results in an increase in the FRCs contractility.

In conclusion, we have shown here that the stromal cells in healthy lungs, kidneys, liver, heart and in naïve lymph nodes keep their fibronectin fibers under high tension, which we now propose to play a major role in maintaining homeostasis in these tissues. In contrast, in either progressive diseases such as cancer, or upon viral infections of lymph nodes, this tensional homeostasis is perturbed. Availability of our fibronectin fiber tension probe thus opens novel possibilities to explore for the first time how the tensional state of fibronectin fibers co-regulates the phenotype of the residing cells, whether these are stromal or immune cells. Usage of this novel tension probe will deepen and expand current knowledge about how cells use mechano-regulated ECM signaling processes to communicate with each other and to synchronize an orchestrated response within multicellular niches. Giving special attention to the mechanical strain state of fibronectin fibers is important, as it not only provides a scaffold for cell adhesion and migration [1,6,60,63], but also has binding sites for a great diversity of growth factors and cytokines, such as IL-7 in lymph nodes [25,59] or the latent complex of TGF-β [42], which can be activated or destroyed by fiber tension [3]. As nothing is known regarding the tensional state of tissue fibers, our proof-of-concept studies further validate that much can be learned from co-staining tissues with our FnBPA5-derived tension probe and other biomarkers, thus paving the way to explore the mechanobiology of tissues under homeostasis and while undergoing pathological transformations. Our discovery that ECM fibers in these healthy and diseased organs exist in distinctly different mechanical tensional states has never been shown before and might play a significant role in the reciprocal crosstalk of cells with their ECM environment and thus steer pathological transformations and disease progression.

Materials and methods

Synthesis and labeling of FnBPA5 and scrambled FnBPA5

FnBPA5 (CGGGQVTTESNLVEFDEESTKGIVTGAVSDHTTVEDTK) and scrambled FnBPA5 (CGSEQEDLTGTKVDFGETIVVNEATETVTSGSTHGTKV) were commercially synthesized (Pichem GmbH, Graz, Austria and Peptide Specialty Laboratories GmbH, Heidelberg, Germany). The N-terminal cysteine was used for further modifications with a Cy5-maleimide fluorescent dye. Lyophilized peptides were dissolved in ultra-pure water (TraceSELECT® quality, Sigma-Aldrich, Buchs, Switzerland) with 10%DMF and stored at –20 °C for further usage.

Preparation of healthy and tumor xenografts cryosections

5 weeks-old female CD1 nude mice were purchased from Charles River (Germany). All the animal experiments were approved by the cantonal authorities and conducted in accordance with the Swiss law for animal protection (license AG 75700). SW2 tumor cells (human lung adenocarcinoma cell line) and Skov3ip tumor cells (ovarian carcinoma cell line), kindly provided by P. Altevogt (German Cancer Research Center, Heidelberg, Germany), were subcutaneously inoculated in both shoulders of the mice (5 Mio. cells in 100 µl PBS per side) after a 5 days acclimatization period. Three weeks after inoculation, the mice were sacrificed and organs were extracted, embedded in cryomedium Tissue-Tek O.C.T. compound

(Sakura, Tokyo, Japan), frozen and cut into 10 µm sections using a histology cryotome (Microm CryoStar HM 560 M, Walldorf, Germany) and placed on Superfrost Plus microscopy slides (Thermo Scientific, USA) and stored at –80 °C until further usage.

Preparation of naïve, LCMV and CpG-infected murine lymph node cryosections

Wild-type C57BL/6 mice were purchased from Janvier Elevage (Le Genest St. Isle, France) and bred under pathogen free conditions. Mice used for the experiments were 6–12 weeks of age and sex-matched. All the animal experiments were approved by the cantonal authorities and conducted in accordance with the Swiss law for animal protection. LCMV-WE was originally obtained from Dr. R.M Zinkernagel (University Hospital Zurich) and propagated in L929 fibroblast cells. CpG oligonucleotide 1668 (TCCATGACGTTCCTGATGCT, phosphorothioate backbone) was synthesized by Mycrosynth (Balgach, Switzerland). Mice were injected with 200 FFU LCMW WE in 50 µl sterile PBS, 5 µg CpG in 50 µl sterile PBS or only 50 µl PBS (control). Mice were sacrificed 8 days after injection and left and right popliteal and inguinal lymph nodes were extracted, weighed and subsequently embedded in Tissue-Tek O.C.T. compound (Sakura, Tokyo, Japan) in Tissue-Tek 4565 disposable vinyl specimen molds (Cryomold Biopsy, Sakura, Tokyo, Japan), frozen and stored at –80 °C before sectioning. Lymph nodes were sectioned using a histology cryotome (Thermo Fisher CryoStar NX70, Thermo Scientific, USA) and placed on Superfrost Plus microscopy slides (Thermo Scientific, USA). 8 µm thick cut sections were then stored at –80 °C until further usage.

Staining of histological tissue sections

Non-fixed tissue cryosections were thawed, washed with 1xPBS, and after a small circle was drawn around the cryosections with a hydrophobic Vector ImmEDGE Hydrophobic Barrier pen (Vector Laboratories, USA), blocked for 30 min with 4% BSA in 1xPBS and subsequently incubated for 60 min with 5 µg/ml Cy5-FnBPA5 or Cy5-labeled scrambled-FnBPA5 (scra-FnBPA5). After a washing step, the tissues were fixed in 4% paraformaldehyde in 1 × PBS for 10 min. Samples were blocked in 1xPBS with 5% goat serum with 0.3 M Glycine for 60 min and incubated with polyclonal rabbit anti fibronectin antibody (ab23750, abcam, Cambridge, UK), or polyclonal rabbit anti α-smooth muscle actin antibody (ab5694, abcam, Cambridge, UK), or monoclonal rat anti reticular fibroblasts and reticular fibers (ER-TR7) antibody (ab51824, abcam, Cambridge, UK), or polyclonal rabbit anti collagen I antibody (ab34710, abcam, Cambridge, UK) overnight at 4 °C. Primary antibody solution was removed and samples were washed with 1xPBS before incubation with secondary goat anti rabbit Alexa 488 (Invitrogen, A11034, Carlsbad, USA) or goat anti rat Alexa 546 (Invitrogen, A11081, Carlsbad, USA) antibody solution for 1 h. After another washing step, some tissues were incubated with 2 µg/ml DAPI for 10 min and further washed before being mounted using DAKO Fluorescence mounting medium (DAKO, Denmark). Once the mounting medium dried, the glass coverslips were sealed with transparent nail polish and imaged with confocal and multiphoton microscopes after 24 h.

Preliminary validation of the specific binding of the FnBPA5 peptide probe to relaxed fibronectin in tissue was performed with mice subcutaneously injected with human prostate carcinoma cell line (PC-3, Cell Lines Service, CLS, Germany) as described in our previous study [21] (Supplementary Fig. S1) and a Cy5-labeled scrambled scra-FnBPA5 derivative was used as a negative control (Supplementary Fig. S6).

Imaging of histological tissue sections

Images presented in Figs. 1 and 2 were acquired using a Leica SP8 confocal and multi-photon microscope. Overviews of the whole tissue sections were acquired with 10× air objective and zoomed-in images of specific area of the tissues were acquired with a 25× water immersion objective. SHG images in Fig. 2B were acquired with a multiphoton laser, excitation at 880 nm. Z-stacks were acquired for every zoomed-in image. The alignment of the multiphoton laser and the confocal laser was verified with the help of TetraSpeck Fluorescent microspheres (Thermo Fisher, USA) and an offset of 3 µm was observed between the 2 lasers. In order to correct for it, this offset was chosen as the z-step size for z-stacks acquisition.

Images showing whole tissue sections in Fig. 3 were acquired using a Nikon TE2000-E epifluorescence microscope equipped with a 40× air objective, individual settings were set depending on the absence of the negative control (scra-FnBPA5, Rabbit anti mouse IgG, Supplementary Fig. S3). Whole tissue sections were visualized by stitching together individual fields of view using the grid/collection stitching plugin in Fiji [61]. Images presented in Fig. S1 were acquired using an Olympus FV-1000 confocal microscope with a 60× oil immersion objective, individual settings were set depending on the absence of the negative control (Cy5-labeled scra-FnBPA5, Rabbit anti mouse IgG, Supplementary Fig. S6 1A). Images presented in Fig. S5 were acquired using a Leica SP-4 confocal microscope with a 63× oil immersion

objective, individual settings were set depending on the absence of the negative control (Cy5-labeled scra-FnBPA5, secondary goat anti rabbit-Alexa488, Supplementary Fig. S6 1B).

Image analysis and spatial proximity analysis

Confocal microscopy images were further analyzed with Fiji and Matlab (Mathworks, Switzerland). For Figs. 1, 2A and 2B, thresholds were determined and applied for each channel in accordance to background signals measured (in these channels) in control tissues incubated solely with secondary antibodies and Cy5-labeled scrambled peptides only.

The spatial proximity analysis in Fig. 2C and 2D was realized with a custom-made Matlab script adapted from Arnoldini et al. [21]. A threshold was first determined with Fiji for every zoomed-in image acquired with 25× water objectives and pixels below this threshold were excluded from the analysis. For each pixel above the intensity threshold in the Cy5-FnBPA5 channel, a 3×3 surrounding evaluation matrix is evaluated in the α-SMA and SHG channel to find one or more proximal pixel above a threshold value in this 3×3 matrix. If at least one proximal pixel is found in this 3×3 evaluation matrix, the evaluated pixel in the Cy5-FnBPA5 channel is marked as a pixel proximal to either α-SMA (Fig. 2C) or SHG (Fig. 2D). The percentages of proximal pixels presented in Fig. 2C and 2D represent the percentages of all pixels found above a threshold in the α-SMA or SHG channels and within a 3×3 defined matrix vicinity for every Cy5-FnBPA5 positive (and above a threshold) pixel. For the kidney tissues, high Cy5-FnBPA5 signal was detected in the glomeruli due to the presence of unstrained plasma fibronectin in the filtering units of the kidney. In order to avoid data misinterpretation caused by averaging the Cy5-FnBPA5 signals over the highly heterogeneous images, the glomeruli areas were first isolated with a mask in every kidney image and the analysis was further run both on the glomeruli-only area and on the images where the glomeruli area had been masked out. For analysis of spatial proximity between Cy5-FnBPA5 channel and SHG channel, the proximity analysis was performed on slices of the stack selected 3 μm apart in z, in order to correct for the physical offset measured between the confocal laser – illuminating the Cy5-FnBPA5 – and the multiphoton laser – creating the SHG signal.

Statistical analysis

For the spatial proximity analysis, statistical significance of the percentages of α-SMA positive pixels and SHG positive pixels in proximity to Cy5-FnBPA5 positive pixels was calculated with a 2-ways ANOVA and a Tukey's correction was applied. Statistical significance was assessed for $p < 0.001$ (***) for Fig. 2C and $p < 0.001$ (***), $p < 0.01$ (**) and $p < 0.05$ (*) for Fig. 2D.

Declaration of competing interest

The authors declare that they have no known competing financial interests or personal relationships that could have appeared to influence the work reported in this paper.

Acknowledgments

We gratefully thank Stefan Imobersteg (PSI), and our lab members Dr. Mamta Chabria, Dr. Isabel Gerber and Chantel Spencer for technical support and discussions, as well as Prof. Cornelia Halin Winter (ETH, D-BIOL) for discussions on IL-7 and the Scientific Center for Optical and Electron Microscopy ScopeM of ETH Zurich, and especially Dr. Justine Kusch from ScopeM for her support with multiphoton imaging.

Funding

This research was supported by ETH Zurich, the Swiss National Science Foundation (SNF Grant CR 32I3_156931 (VV), SNF-ANR Grant 310030E-164284 (VV), SNF Grant 31003A-175839 (VV) and SNF Grant 310030_179342 (MB)), as well as by the Wyss Center Zurich.

Author contributions

S.A., A.M., C.M.F., M.B. and V.V. designed tumor tissue experiments and S.A., D.J., A.O. and V.V. designed lymph node experiments. A.M. conducted the in vivo work for the tumor-xenografted mice, as well as organ excretion. C.M.F. and S.A. conducted all the healthy and tumor tissue stains, imaging and analysis. D.J. conducted the in vivo work for the mice lymph nodes experiment, as well as organ excretion of lymph nodes. S.A. weighed, sectioned and stained the lymph nodes. S.A., C.M.F., D.J., and V. V. wrote the manuscript. All authors read and approved the manuscript.

Data and materials availability

All relevant data are available from the authors upon request.

Appendix A. Supplementary data

Supplementary data to this article can be found online at https://doi.org/10.1016/j.mbplus.2020.100046.

Received 15 May 2020;
Received in revised form 9 July 2020;
Accepted 9 July 2020
Available online 17 July 2020

Keywords:
Extracellular matrix;
Fibronectin;
Mechanobiology;
Cancer;
Lymph node;
Virus infection

These authors contributed equally to this work.

Abbreviations used:
α-SMA, alpha smooth muscle actin; CAFs, cancer associated fibroblasts; CLEC-2, C-type Lectin Receptor; DCs, dendritic cells; ECM, extracellular matrix; FRCs, fibroblastic reticular cells; IHC, immunohistochemistry; IL-7, Interleukin 7; LCMV, lymphocytic choriomeningitis virus; MMPs, matrix metalloproteinases; PDPN, podoplanin; SHG, second harmonic generation; TGF-β, Transforming Growth Factor-beta.

References

[1] R.O. Hynes, The extracellular matrix: not just pretty fibril, Science. 326 (2009) 1216–1219, https://doi.org/10.1126/science.1176009.
[2] R.V. Iozzo, M.A. Gubbiotti, Extracellular matrix: the driving force of mammalian diseases, Matrix Biol. 71–72 (2018) 1–9, https://doi.org/10.1016/j.matbio.2018.03.023.
[3] V. Vogel, Unraveling the mechanobiology of extracellular matrix, Annu. Rev. Physiol. 80 (2018) 353–387, https://doi.org/10.1146/annurev-physiol-021317-121312.
[4] J.D. Humphrey, E.R. Dufresne, M.A. Schwartz, Mechanotransduction and extracellular matrix homeostasis, Nat. Rev. Mol. Cell Biol. 15 (2014) 802–812, https://doi.org/10.1038/nrm3896.
[5] C. Bonnans, J. Chou, Z. Werb, Remodelling the extracellular matrix in development and disease, Nat. Rev. Mol. Cell Biol. 15 (2014) 786–801, https://doi.org/10.1038/nrm3904.
[6] B. Hubbard, J.A. Buczek-Thomas, M.A. Nugent, M.L. Smith, Fibronectin fiber extension decreases cell spreading and migration, J. Cell. Physiol. 231 (2016) 1728–1736, https://doi.org/10.1002/jcp.25271.
[7] W.R. Legant, C.S. Chen, V. Vogel, Force-induced fibronectin assembly and matrix remodeling in a 3D microtissue model of tissue morphogenesis, Integr. Biol. 4 (2012) 1164–1174, https://doi.org/10.1039/c2ib20059g.
[8] C. Walker, E. Mojares, A. Del Río Hernández, Role of extracellular matrix in development and cancer progression, Int. J. Mol. Sci. 19 (2018)https://doi.org/10.3390/ijms19103028.
[9] B. Piersma, M.K. Hayward, V.M. Weaver, Fibrosis and cancer: a strained relationship, Biochim. Biophys. Acta Rev. Cancer 2020 (1873)https://doi.org/10.1016/j.bbcan.2020.188356.
[10] J.J. Northey, L. Przybyla, V.M. Weaver, Tissue force programs cell fate and tumor aggression, Cancer Discov. 7 (2017) 1224–1237, https://doi.org/10.1158/2159-8290.CD-16-0733.
[11] G. Baneyx, L. Baugh, V. Vogel, Coexisting conformations of fibronectin in cell culture imaged using fluorescence resonance energy transfer, Proc. Natl. Acad. Sci. 98 (2001) 14464–14468, https://doi.org/10.1073/pnas.251422998.
[12] J.I. Lopez, I. Kang, W.K. You, D.M. McDonald, V.M. Weaver, In situ force mapping of mammary gland transformation, Integr. Biol. 3 (2011) 910–921, https://doi.org/10.1039/c1ib00043h.
[13] M. Plodinec, M. Loparic, C.A. Monnier, E.C. Obermann, R. Zanetti-Dallenbach, P. Oertle, J.T. Hyotyla, U. Aebi, M. Bentires-Alj, R.Y.H. Lim, C.A. Schoenenberger, The nanomechanical signature of breast cancer, Nat. Nanotechnol. 7 (2012) 757–765, https://doi.org/10.1038/NNANO.2012.167.
[14] K.R. Levental, H. Yu, L. Kass, J.N. Lakins, M. Egeblad, J.T. Erler, S.F.T. Fong, K. Csiszar, A. Giaccia, W. Weninger, M. Yamauchi, D.L. Gasser, V.M. Weaver, Matrix crosslinking forces tumor progression by enhancing integrin signaling, Cell. 139 (2009) 891–906, https://doi.org/10.1016/j.cell.2009.10.027.
[15] J.L. Leight, A.P. Drain, V.M. Weaver, Extracellular matrix remodeling and stiffening modulate tumor phenotype and treatment response, Annu. Rev. Cancer Biol. 1 (2017) 313–334, https://doi.org/10.1146/annurev-cancerbio-050216-034431.
[16] D. Duscher, Z.N. Maan, V.W. Wong, R.C. Rennert, M. Januszyk, M. Rodrigues, M. Hu, A.J. Whitmore, A.J. Whittam, M.T. Longaker, G.C. Gurtner, Mechanotransduction and fibrosis, J. Biomech. 47 (2014) 1997–2005, https://doi.org/10.1016/j.jbiomech.2014.03.031.
[17] B. Hinz, S.H. Phan, V.J. Thannickal, M. Prunotto, A. Desmoulière, J. Varga, O. De Wever, M. Mareel, G. Gabbiani, Recent developments in myofibroblast biology, Am. J. Pathol. 180 (2012) 1340–1355, https://doi.org/10.1016/j.ajpath.2012.02.004.
[18] J.L. Astarita, V. Cremasco, J. Fu, M.C. Darnell, J.R. Peck, J. M. Nieves-Bonilla, K. Song, Y. Kondo, M.C. Woodruff, A. Gogineni, L. Onder, B. Ludewig, R.M. Weimer, M.C. Carroll, D.J. Mooney, L. Xia, S.J. Turley, The CLEC-2-podoplanin axis controls the contractility of fibroblastic reticular cells and lymph node microarchitecture, Nat. Immunol. 16 (2015) 75–84, https://doi.org/10.1038/ni.3035.
[19] S.E. Acton, C. Reis e Sousa, Dendritic cells in remodeling of lymph nodes during immune responses, Immunol. Rev. 271 (2016) 221–229, https://doi.org/10.1111/imr.12414.
[20] A.L. Fletcher, S.E. Acton, K. Knoblich, Lymph node fibroblastic reticular cells in health and disease, Nat. Rev. Immunol. 15 (2015) 350–361, https://doi.org/10.1038/nri3846.
[21] S. Arnoldini, A. Moscaroli, M. Chabria, M. Hilbert, S. Hertig, R. Schibli, M. Béhé, V. Vogel, Novel peptide probes to assess the tensional state of fibronectin fibers in cancer, Nat. Commun. 8 (2017)https://doi.org/10.1038/s41467-017-01846-0.

[22] M. Chabria, S. Hertig, M.L. Smith, V. Vogel, Stretching fibronectin fibres disrupts binding of bacterial adhesins by physically destroying an epitope, Nat. Commun. 1 (2010) https://doi.org/10.1038/ncomms1135.
[23] S. Hertig, M. Chabria, V. Vogel, Engineering mechanosensitive multivalent receptor–ligand interactions: why the nanolinker regions of bacterial adhesins matter, Nano Lett. 12 (2012) 5162–5168, https://doi.org/10.1021/nl302153h.
[24] M.E. Vega, J.E. Schwarzbauer, Collaboration of fibronectin matrix with other extracellular signals in morphogenesis and differentiation, Curr. Opin. Cell Biol. 42 (2016) 1–6, https://doi.org/10.1016/j.ceb.2016.03.014.
[25] D. Ortiz Franyuti, M. Mitsi, V. Vogel, Mechanical stretching of fibronectin fibers upregulates binding of interleukin-7, Nano Lett. 18 (2018) 15–25, https://doi.org/10.1021/acs.nanolett.7b01617.
[26] A. Krammer, H. Lu, B. Isralewitz, K. Schulten, V. Vogel, Forced unfolding of the fibronectin type III module reveals a tensile molecular recognition switch, Proc. Natl. Acad. Sci. U. S. A. 96 (1999) 1351–1356, https://doi.org/10.1073/pnas.96.4.1351.
[27] L. Cao, J. Nicosia, J. Larouche, Y. Zhang, H. Bachman, A.C. Brown, L. Holmgren, T.H. Barker, Detection of an integrin-binding mechanoswitch within fibronectin during tissue formation and fibrosis, ACS Nano 11 (2017) 7110–7117, https://doi.org/10.1021/acsnano.7b02755.
[28] K.E. Kubow, R. Vukmirovic, L. Zhe, E. Klotzsch, M.L. Smith, D. Gourdon, S. Luna, V. Vogel, Mechanical forces regulate the interactions of fibronectin and collagen I in extracellular matrix, Nat. Commun. 6 (2015)https://doi.org/10.1038/ncomms9026.
[29] B. Li, C. Moshfegh, Z. Lin, J. Albuschies, V. Vogel, Mesenchymal stem cells exploit extracellular matrix as mechanotransducer, Sci. Rep. 3 (2013).
[30] E.L. George, E.N. Georges-Labouesse, R.S. Patel-King, H. Rayburn, R.O. Hynes, Defects in mesoderm, neural tube and vascular development in mouse embryos lacking fibronectin, Development. 119 (1993) 1079–1097.
[31] J.P. Wang, A. Hielscher, Fibronectin: how its aberrant expression in tumors may improve therapeutic targeting, J. Cancer 8 (2017) 674–682, https://doi.org/10.7150/jca.16901.
[32] J.A. Eble, S. Niland, The extracellular matrix in tumor progression and metastasis, Clin. Exp. Metastasis 36 (2019) 171–198, https://doi.org/10.1007/s10585-019-09966-1.
[33] T.C. Lin, C.-H. Yang, L.-H. Cheng, W.-T. Chang, Y.-R. Lin, H.-C. Cheng, Fibronectin in cancer: friend or foe, Cells 9 (2019)https://doi.org/10.3390/cells9010027.
[34] G. Efthymiou, A. Saint, M. Ruff, Z. Rekad, D. Ciais, E. Van Obberghen-Schilling, Shaping up the tumor microenvironment with cellular fibronectin, Front. Oncol. 10 (2020)https://doi.org/10.3389/fonc.2020.00641.
[35] B. Hinz, D. Lagares, Evasion of apoptosis by myofibroblasts: a hallmark of fibrotic diseases, Nat. Rev. Rheumatol. 16 (2020) 11–31, https://doi.org/10.1038/s41584-019-0324-5.
[36] R. Kalluri, The biology and function of fibroblasts in cancer, Nat. Rev. Cancer 16 (2016) 582–598, https://doi.org/10.1038/nrc.2016.73.
[37] T. Lammers, F. Kiessling, W.E. Hennink, G. Storm, Drug targeting to tumors: principles, pitfalls and (pre-) clinical progress, J. Control. Release 161 (2012) 175–187, https://doi.org/10.1016/j.jconrel.2011.09.063.
[38] L. Cao, M.K. Zeller, V.F. Fiore, P. Strane, H. Bermudez, T.H. Barker, Phage-based molecular probes that discriminate force-induced structural states of fibronectin in vivo, Proc. Natl. Acad. Sci. 109 (2012) 7251–7256, https://doi.org/10.1073/pnas.1118088109.
[39] E. Scandella, B. Bolinger, E. Lattmann, S. Miller, S. Favre, D. R. Littman, D. Finke, S.A. Luther, T. Junt, B. Ludewig, Restoration of lymphoid organ integrity through the interaction of lymphoid tissue–inducer cells with stroma of the T cell zone, Nat. Immunol. 9 (2008) 667–675, https://doi.org/10.1038/ni.1605.
[40] A. Desmoulière, Factors influencing myofibroblast differentiation during wound healing and fibrosis, Cell Biol. Int. 19 (1995) 471–476, https://doi.org/10.1006/cbir.1995.1090.
[41] D.A. Rytand, The number and size of mammalian glomeruli as related to kidney and to body weight, with methods for their enumeration and measurement, Am. J. Anat. 62 (1938) 507–520, https://doi.org/10.1002/aja.1000620406.
[42] B. Hinz, The extracellular matrix and transforming growth factor-beta1: tale of a strained relationship, Matrix Biol. 47 (2015) 54–65, https://doi.org/10.1016/j.matbio.2015.05.006.
[43] S. Roth, I. Freund, Optical second-harmonic scattering in rat-tail tendon, Biopolymers. 20 (1981) 1271–1290, https://doi.org/10.1002/bip.1981.360200613.
[44] G.C. Cox, F. Manconi, E. Kable, Second harmonic imaging of collagen in mammalian tissue, Proc. SPIE 4620 (2002) 148–156, https://doi.org/10.1117/12.470689.
[45] A. Filippi, E.D. Sasso, L. Iop, A. Armani, M. Gintoli, M. Sandri, G. Gerosa, F. Romanato, G. Borile, Multimodal label-free ex vivo imaging using a dual-wavelength microscope with axial chromatic aberration compensation, J. Biomed. Opt. 23 (2018)https://doi.org/10.1117/1.JBO.23.9.091403.
[46] M. Sixt, N. Kanazawa, M. Selg, T. Samson, G. Roos, D.P. Reinhardt, R. Pabst, M.B. Lutz, L. Sorokin, The conduit system transports soluble antigens from the afferent lymph to resident dendritic cells in the T cell area of the lymph node, Immunity. 22 (2005) 19–29, https://doi.org/10.1016/j.immuni.2004.11.013.
[47] R. Malik, P.I. Lelkes, E. Cukierman, Biomechanical and biochemical remodeling of stromal extracellular matrix in cancer, Trends Biotechnol. 33 (2015) 230–236, https://doi.org/10.1016/j.tibtech.2015.01.004.
[48] M.W. Conklin, J.C. Eickhoff, K.M. Riching, C.A. Pehlke, K.W. Eliceiri, P.P. Provenzano, A. Friedl, P.J. Keely, Aligned collagen is a prognostic signature for survival in human breast carcinoma, Am. J. Pathol. 178 (2011) 1221–1232, https://doi.org/10.1016/j.ajpath.2010.11.076.
[49] P. Friedl, S. Alexander, Cancer invasion and the microenvironment: plasticity and reciprocity, Cell. 147 (2011) 992–1009, https://doi.org/10.1016/j.cell.2011.11.016.
[50] K. Wang, F. Wu, B.R. Seo, C. Fischbach, W. Chen, L. Hsu, D. Gourdon, Breast cancer cells alter the dynamics of stromal fibronectin-collagen interactions, Matrix Biol. 60–61 (2017) 86–95, https://doi.org/10.1016/J.MATBIO.2016.08.001.
[51] G.A. Conlon, G.I. Murray, Recent advances in understanding the roles of matrix metalloproteinases in tumour invasion and metastasis, J. Pathol. 247 (2019) 629–640, https://doi.org/10.1002/path.5225.
[52] J.E. Gretz, C.C. Norbury, A.O. Anderson, A.E.I. Proudfoot, S. Shaw, Lymph-borne chemokines and other low molecular weight molecules reach high endothelial venules via specialized conduits while a functional barrier limits access to the lymphocyte microenvironments in lymph node cortex, J. Exp. Med. 192 (2000) 1425–1439, https://doi.org/10.1084/jem.192.10.1425.
[53] A.J. Meinel, K.E. Kubow, E. Klotzsch, M. Garcia-Fuentes, M. L. Smith, V. Vogel, H.P. Merkle, L. Meinel, Optimization strategies for electrospun silk fibroin tissue engineering scaffolds, Biomaterials. 30 (2009) 3058–3067, https://doi.org/10.1016/j.biomaterials.2009.01.054.

[54] M. Antia, G. Baneyx, K.E. Kubow, V. Vogel, Fibronectin in aging extracellular matrix fibrils is progressively unfolded by cells and elicits an enhanced rigidity response, Faraday Discuss. 139 (2008) 229–249.

[55] C.Y. Yang, T.K. Vogt, S. Favre, L. Scarpellino, H.Y. Huang, F. Tacchini-Cottier, S.A. Luther, Trapping of naive lymphocytes triggers rapid growth and remodeling of the fibroblast network in reactive murine lymph nodes, Proc. Natl. Acad. Sci. 111 (2014) E109–E118, https://doi.org/10.1073/pnas.1312585111.

[56] R.S. Chu, O.S. Targoni, A.M. Krieg, P.V. Lehmann, C.V. Harding, CpP oligodeoxynucleotides act as adjuvants that switch on T helper 1 (Th1) immunity, J. Exp. Med. 186 (1997) 1623–1631, https://doi.org/10.1084/jem.186.10.1623.

[57] T.J. Fry, E. Connick, J. Falloon, M.M. Lederman, D.J. Liewehr, J. Spritzler, S.M. Steinberg, L.V. Wood, R. Yarchoan, J. Zuckerman, A. Landay, C.L. Mackall, A potential role for interleukin-7 in T-cell homeostasis, Blood. 97 (2001) 2983–2990, https://doi.org/10.1182/blood.V97.10.2983.

[58] C.D. Surh, J. Sprent, Homeostasis of naive and memory T cells, Immunity. 29 (2008) 848–862, https://doi.org/10.1016/j.immuni.2008.11.002.

[59] A. Ariel, R. Hershkoviz, L. Cahalon, D.E. Williams, S.K. Akiyama, K.M. Yamada, C. Chen, R. Alon, T. Lapidot, O. Lider, Induction of T cell adhesion to extracellular matrix or endothelial cell ligands by soluble or matrix-bound interleukin-7, Eur. J. Immunol. 27 (1997) 2562–2570, https://doi.org/10.1002/eji.1830271015.

[60] R.O. Hynes, K.M. Yamada, Fibronectins: multifunctional modular glycoproteins, J. Cell Biol. 95 (1982) 369–377, https://doi.org/10.1083/jcb.95.2.369.

[61] S. Preibisch, S. Saalfeld, P. Tomancak, Globally optimal stitching of tiled 3D microscopic image acquisitions, Bioinformatics. 25 (2009) 1463–1465, https://doi.org/10.1093/bioinformatics/btp184.

[62] E. Klotzsch, M. Smith, K.E. Kubow, S. Muntwyler, W. Little, F. Beyeler, D. Gourdon, B.J. Nelson, V. Vogel, Fibronectin forms the most extensible biological fibers displaying switchable force-exposed cryptic binding sites, Proc. Natl. Acad. Sci. U. S. A. 106 (43) (2009) 18267–18272, https://doi.org/10.1073/pnas.0907518106.

[63] M. Mitsi, M.M.P. Schulz, E. Gousopoulos, A.M. Ochsenbein, M. Detmar, V. Vogel, Walking the line: a fibronectin fiber-guided assay to probe early steps of (lymph) angiogenesis, PLos One 10 (12) (2015)https://doi.org/10.1371/journal.pone.0145210.